A Cavity-backed Slot Antenna with Dual-polarized In-band RCS Reduction Using Polarization Conversion Metasurface

Bing Han, Xianglin Kong, Lei Zhao, *Senior Member, IEEE,* Jun Wang, *Member, IEEE,* Ming Cheng, *Member, IEEE,* Zhongxiang Shen, *Fellow, IEEE*

***Abstract*—In this letter, a cavity-backed slot (CBS) array with wideband radiation and low in-band dual-polarized scattering is presented. The radiator of the wideband antenna element is a metallic cavity, which is fed by a microstrip line on the substrate. The polarization conversion metasurface (PCM) is designed to reduce the in-band radar cross section (RCS) of the antenna array. Its operating frequency range covers the antenna impedance bandwidth from 5.5 to 7.7 GHz. Simulated and measured results show that the low-scattering antenna has a -10 dB impedance bandwidth of 33.3%, and a stable realized gain greater than 13 dBi. Furthermore, the array has a dual-polarized RCS reduction higher than 10 dB from 5.4 to 8.5 GHz compared with the reference antenna. A prototype is fabricated and tested, and measured results are in good agreement with the simulation results.**

***Index Terms*—Radar cross section (RCS), cavity-backed slot (CBS) antenna, polarization conversion metasurface.**

I. INTRODUCTION

As an obvious scattering source on military targets, the radar antenna greatly increases the exposure risk [1], [2]. Reducing the radar cross-section (RCS) of antennas has become an important study since the last century [3], [4]. In recent years, low scattering techniques for wideband antennas have become more and more important.

In order to balance the stable radiation performance and low scattering characteristics of antennas, several approaches have been developed to reduce their RCS. Among these measures, placing an absorbing structure around the antenna is a proven method [5], [6], [7]. However, the distance from the antenna to absorber should be carefully arranged to avoid degrading its radiation energy [8], [9], [10], Therefore, the application method of these schemes is limited. An improved idea is to share the metal backplane for the absorbing structure and antenna layer [11], [12], [13]. Because the resistive layer is designed to retain a transmission window for antenna radiation on the notch band for broadband absorption, the above structures make the in-band RCS of the antenna structure to be approximately the same as that of the reference antenna. Phase cancellation technique has also been explored to design polarization conversion metasurface (PCM), which can be arranged adjacent with the antenna to reduce the RCS of antenna [14], [15], [16]. An alternative method is to integrate patch antennas into a metasurface with inherent phase-cancellation ability [17], [18]. Nevertheless, this approach is generally limited to narrowband use. Meeting the demands of complex environments requires a stealth antenna that combines wideband operation with low scattering. This calls for a new antenna design featuring broadband performance and in-band, polarization-independent stealth.

In consideration of the preceding studies and aforementioned analysis, a considerable ability of PCM is that it has little effect on the antenna's radiation, even when the distance between antenna and PCM is close. It can be posited that the utilization of PCM to reduce the in-band RCS of wideband antenna arrays is a promising approach. Inspired by the predecessors' research, a cavity-backed slot (CBS) array based on PCM and shared-structure is proposed to achieve broadband and low in-band scattering performance. Compared to previous studies, our study has the following advantages.

1) The shared-aperture structure ensures that the antenna has a wide bandwidth and high gain.
2) The frequency range of RCS reduction covers the operating frequency range of CBS antenna array fully.
3) The RCS reduction ability is realizable for both co-polarized and cross-polarized incident plane wave.

II. DESIGN OF LOW-SCATTERING CBS ANTENNA

Fig. 1 illustrates the working and scattering mechanism of the proposed array, which consists of two dielectric substrate layers and a metal layer. The proposed antenna array is a 2×4 array with *x*-polarized radiation and wide operating frequency. The PCM working band is designed based on the antenna's working band strictly. For radiation, the electromagnetic waves generated by the antenna array pass through the top layer with rectangle gap. For being scanned

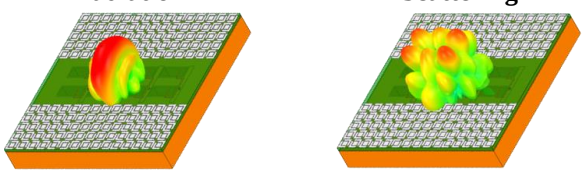

(a) (b)

Fig. 1. Schematic diagram of the antenna, (a) radiation state, (b) scattering state.

This work was supported in part by the Postgraduate Research and Practice Innovation Program of Jiangsu Province under Grant KYCX25_2844; and in part by Graduate Innovation Program of China University of Mining and Technology under Grant 2025WLKXJ108, (Corresponding author: L. Zhao).

B. Han, X. Kong, L. Zhao, J. Wang, and M. Cheng are with the School of Information and Control Engineering, China University of Mining and Technology, Xuzhou, China (e-mail: bhan@cumt.edu.cn, xlkong@cumt.edu.cn, leizhao@cumt.edu.cn, jun-wang@cumt.edu.cn, ming_cheng@cumt.edu.cn).

Z. Shen is with the Beijing Institute of Technology, Jiaxing, Zhejiang, China 314019 (e-mail: shenzx@bit.edu.cn).

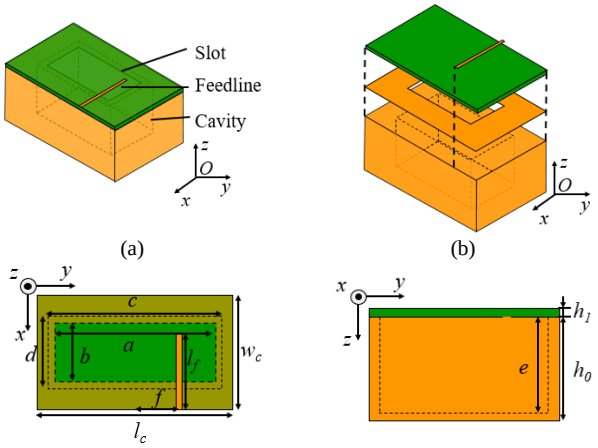

Fig. 2. Structure of antenna cell, (a) antenna element, (b) four-layer structure, (c) top view, (d) side view.

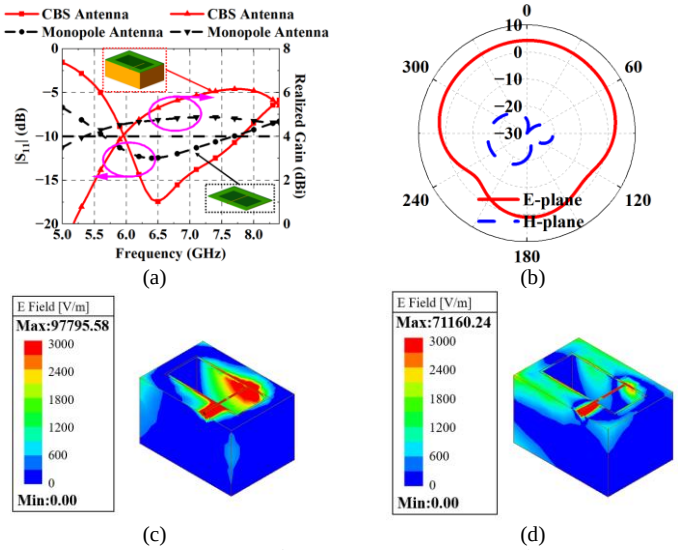

Fig.3. Radiation characteristic of CBS antenna and electric field amplitude distributions of two resonant frequencies, (a) $|S_{11}|$ and realized gain of two kinds antenna element, (b) radiation directivity of CBS antenna element. (c) at f_c = 6.5 GHz, (d) at f_c = 7.5 GHz.

state, a scattering phenomenon is observed at backward direction. Above all, the antenna capabilities contribute to stable radiation and reduced probability of detection in band.

A. Design of Antenna Element

Fig. 2 illustrates the designed CBS antenna element consisted by four-layer structure. As shown in Fig. 2(b), the metal layer is formed by excavating a cavity within the entire metallic body, which serves as the radiating cavity of the antenna element. The dielectric layer formed by a lossy substrate F4BM ($\varepsilon_r = 2.2$, $tan\delta = 0.0009$) and printed copper on both sides. The bottom layer is the radiation gap and the top layer is microstrip line of the antenna element, respectively. The final optimized dimensions of the CBS antenna element are a = 21.8 mm, b = 11.6 mm, c = 23.6 mm, d = 13.6 mm, e = 17 mm, f = 6.3 mm, h_0 = 18 mm, h_1 = 0.8 mm, l_c = 29 mm, w_c = 20 mm, l_f = 12 mm, w_f = 0.66 mm, respectively.

Fig. 3 describes the radiation ability of antenna. In contrast to a conventional monopole, the CBS antenna has a common-

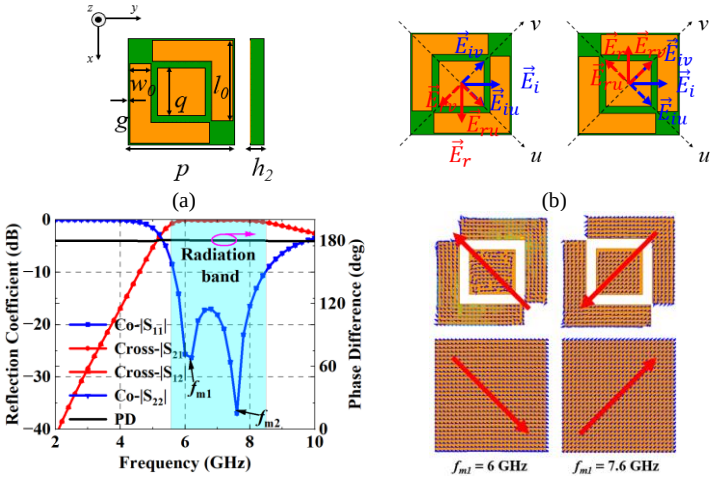

Fig. 4. PCM Structure and its polarized conversion ability, (a) structure, (b) mechanism of Cell 0 and Cell 1, (c) polarized conversion ability, (d) magnetic resonance of PCM cell at 6 GHz and 7.6 GHz.

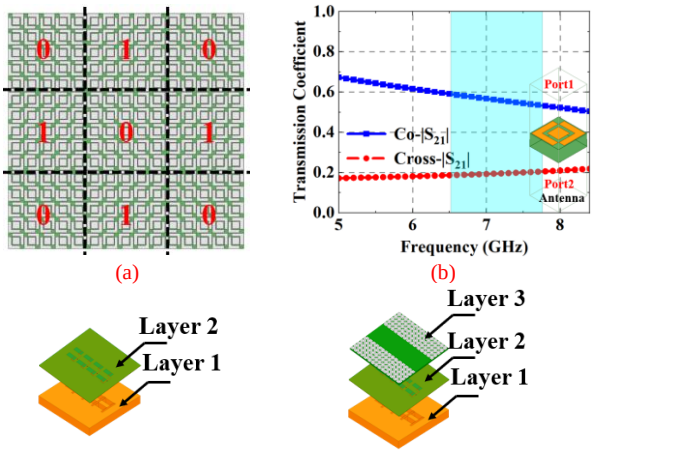

Fig. 5. Structure evolution of low RCS antenna array, (a) structure of initial PCM metasurface, (b) transmission coefficient of PCM without ground

aperture design with a back cavity. This structure ensures improved impedance matching and higher gain, which collectively yield a lower scattering signature while maintaining favorable radiation characteristics. Fig. 3(a) demonstrates that the designed antenna element operates within a bandwidth of 6-7.8 GHz. Fig. 3(b) presents the radiation pattern at the resonant frequency f_0 = 6.5 GHz. At f_0 = 6.5 GHz, the main polarization significantly surpasses the cross polarization by 20 dB. Within the frequency range from 6 to 7.8 GHz, the maximum gain of the antenna reached 6 dBi. At 6.5 GHz, the electric field concentrates in the gap of the metal back cavity, while at 7.5 GHz, it concentrates along the microstrip line. This confirms resonance at both frequencies. The stronger field amplitude in the cavity gap identifies it as the primary resonant point. Thus, a 26% relative bandwidth and good radiation directivity together make the proposed structure an effective broadband antenna.

B. Design of PCM Cell

In order to meet the demand of low RCS in the whole operating band of antenna. Fig. 4(a) presents a PCM structure

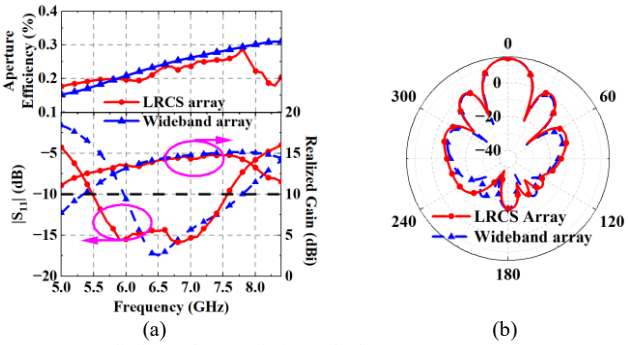

(a) (b)

Fig. 6. Radiation characteristics of the antenna array, (a) Aperture efficiency, $|S_{11}|$ and realized gain, (b) directionality at 6.5GHz.

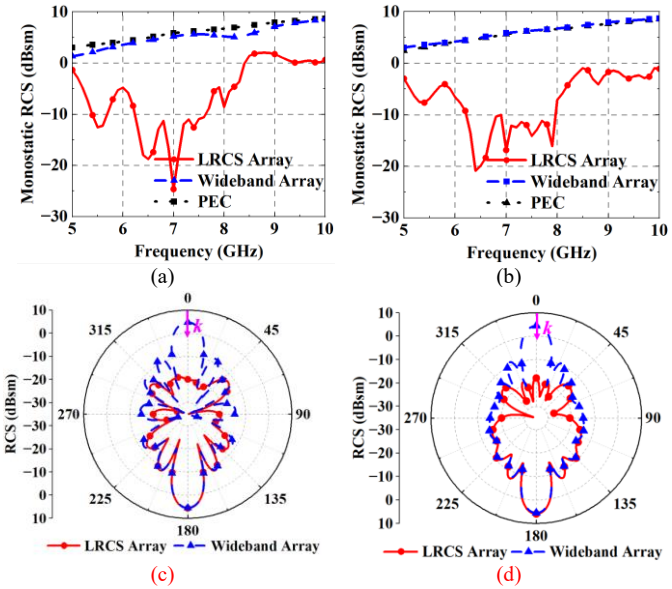

(a) (b) (c) (d)

Fig. 7. Scattering characteristics of the antenna for incident waves with different polarization modes, (a) MRCS for *x*-polarized wave, (b) MRCS for *y*-polarized wave, (c) BRCS for *x*-polarized wave, (d) BRCS for *y*-polarized wave.

named Cell 1 based on F4BM as the dielectric substrate. A 90° rotation of Cell 1 results in Cell 0 as shown in Fig.4(b). Copper layers with a thickness of t = 0.035 mm are printed on both sides. The upper layer is etched to form a pair of right-angle patterns and a square patch, which together constitute the structure layer. The other dimensions of the CBS antenna element are p = 10 mm, l_0 = 7.4 mm, w_0 = 2.1 mm, q = 4.8 mm, h_2 = 3 mm, g = 0.1 mm, respectively.

Fig. 4(c) presents the polarization conversion coefficient and reflection phase difference of two kinds of PCM cell. The design of polarized converse band depends on the working band of antenna element, which ensures the RCS reduction band covers the same frequency range. In this design, two kinds of circulating currents are formed on the top metal structure and the bottom ground plane at f_{m1} = 6.0 GHz and f_{m2} = 7.6 GHz, which are excited magnetic resonance as shown in Fig. 4(d). Within the frequency range of 5.8-8.2 GHz, the co-polarized reflection coefficients are less than -10 dB, and the cross-polarized reflection coefficients are greater than -1dB for both two kinds of PCM cells. In the meanwhile, the phase differences of them keep 180 deg. It is proved that the designed PCM has an excellent polarized conversion ability.

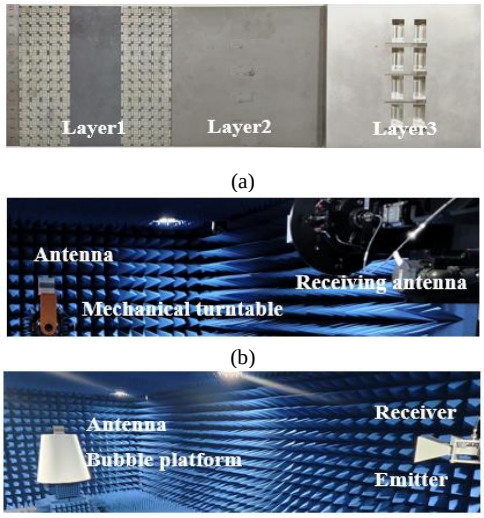

(a) (b) (c)

Fig. 8. Measurement of the proposed low RCS CBS array. (a) Prototype structure of two dielectric layers and metal cavity. (b) Radiation field measurement environment. (c) RCS measurement environment.

C. Design of Low-RCS Antenna Array

Fig. 5 shows the structure evolution of low RCS antenna array. The closely arranged antenna elements guide the arrangement of PCM cells. As shown in Fig. 5(a), Cell 1 and Cell 0 form a 5×5 checkerboard grid on the final PCM layer. Fig. 5(b) shows that this layout adversely affects radiation from over half the antennas within the band. Performance is improved by removing the middle rectangular strip. Fig. 5(c) shows the initial wideband antenna, which serves as the reference antenna for the low-scattering antenna in Fig. 5(d). Fig. 6 shows the radiation performance of the wideband CBS antenna array and the low-scattered CBS antenna array. It should be mentioned that some power is inevitably dissipated due to the fact that the radiation of the antenna needs to pass through the metasurface, which slightly decreases the aperture efficiency of the CBS array. Moreover, the realized gain of low-scattered antenna is improved in 5.5-6.0 GHz. The main lobe gain remains stable at f_0 = 6.5 GHz. In conclusion, the introduction of the PCM has little influence on the antenna radiation performance. In conclusion, the low-scattered CBS antenna array preserves the advantage of the initial designed antenna: wideband, high gain and excellent directivity.

The monostatic and bistatic RCS of both antennas under matched load are shown in Fig. 7, benchmarked against a metal plate of equal area. The MRCS results in Figs. 7(a) and 7(b) demonstrate that the proposed antenna reduces RCS by over 10 dB from 5.8 to 8 GHz for co-polarization, with cross-polarization performance covering this full band as well. This represents a key improvement over the initial array, as the low-scattering design now achieves significant RCS reduction across the complete operating band for both polarizations. As shown in Fig. 7(c) and 7(d), it achieves RCS reduction within ±45° for both x- and y-polarized waves for the normal incident plane wave at 6.5 GHz. Within ±20° range, the reduction exceeds 10 dB. Consequently, the proposed low RCS CBS array results in significantly reduced scattering relative to the reference wideband array.

TABLE I

ANTENNA PERFORMANCE COMPARISON

Ref.	Mechanism	Electronic Size (λ_0^3)	Impedance bandwidth	In-band RCSR proportion Co-pol.	Cross-pol.	Aperture Efficiency	Peak gain (dBi)
[3]	Absorption	5.6×5.6×1.16	20.0%	0@>10dB	100%@>10dB	70%	21.5
[4]	Phase cancellation	4.4×4.4×0.15	36.7%	100%@>8dB	100%@>0dB	77%	20.0
[10]	Absorption	5.2×9.5×0.4	16.2%	0@>10dB	100%@>10dB	/	14.9
[12]	Phase cancellation	2.2×2.2×0.8	10.1%	60%@>10dB	60%@>10dB	62.5%	13.0
This work	Phase cancellation	3.3×3.3×0.45	33.3%	100%@>10dB	100%@>10dB	23.1%	15.0

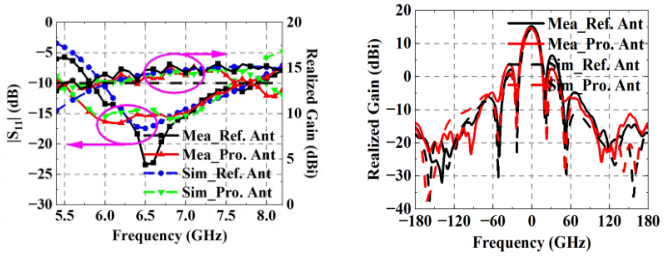

(a) (b)

Fig. 9. Measurement radiation characteristics of the prototype array, (a) $|S_{11}|$ and realized gain of reference antenna and proposed antenna, (b) directionality at 6.5 GHz of reference antenna and low RCS antenna.

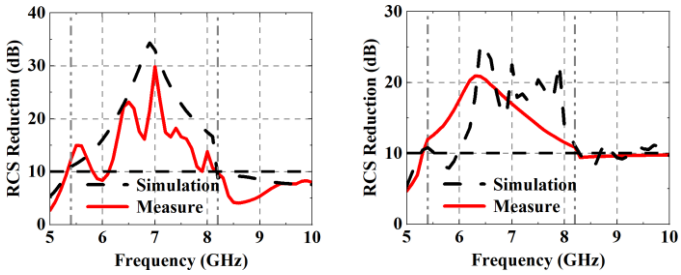

(a) (b)

Fig. 10. Measurement RCS reduction of the prototype array, (a) MRCS for *x*-polarized wave, (b) MRCS for *y*-polarized wave.

III. FABRICATION AND MEASUREMENTS

In order to verify the scattering and radiation performance of the designed antenna array, we fabricated and measured a prototype, as shown in Fig. 8(a). In this prototype, the two layers of dielectric materials are closely stacked with the bottom metal cavity structure through the side adhesive tape. Fig. 8(b) presents the radiation characteristics were measured by placing the prototype on the horizontal mechanical turntable using the standard gain comparison method. The experimental test adopted the time-domain gated function to eliminate environmental interference. Fig. 8(c) shows the RCS measure environment, an antenna prototype with matched load was placed on the bubble and a pair of horn was connected to a vector network analyzer to obtain the RCS value of the prototype.

A. Radiation Performance of Antenna Array

Fig. 9 shows the measurement and simulation results of the radiation of the low-scattering antenna and the wideband antenna. The slight deformation caused by the assembly of the antenna has a minor impact on the measurement results. The impedance bandwidth of the low-scattering antenna and wideband antenna are similar to simulation results. $|S_{11}|$ below −10 dB is from 5.5 to 7.7 GHz for the proposed antenna and the realized gain remains at least 13 dBi in this frequency range. At the typical resonant point f_0 = 6.5 GHz of the wideband antenna, the main lobes of the measured and simulated patterns are basically consistent. These results prove that the proposed antenna design is effective and feasible.

B. Scattering Performance of Antenna Array

Fig. 10 analyzed and calculated RCS reduction of the low-scattering antenna with respect to the wideband antenna. Similarly, the minor deformations of the antenna assembly have some influence on the measurement results. Both the measurement results and the simulation results maintained an RCS reduction of over than 10 dB within the frequency range of 5.4-8.2 GHz. It can be proved that the designed low RCS antenna has a dual-polarized RCS reduction characteristic covering the entire working band.

Table I compares this work with existing methods for in-band RCS reduction. The proposed metasurface antenna achieves a superior trade-off, integrating wideband operation with uniform RCS reduction via phase cancellation. Key results include a 33.3% impedance bandwidth, a 15.0 dBi peak gain, and a sustained in-band RCS reduction of over 10 dB for both polarizations, ensuring reliable stealth performance.

IV. CONCLUSION

This paper proposes a broadband low-scattering antenna based on a polarization conversion metasurface. The design integrates a PCM checkerboard layout with a staggered antenna array to reduce in-band RCS while preserving radiation performance. Simulations agree well with measurements. The antenna achieves a 33.3% impedance bandwidth and a stable gain above 13 dBi with favorable directivity. A monostatic RCS reduction is maintained from 5.4 to 8.2 GHz, covering the full operating band, while the bistatic RCS exhibits a distinct backscattering null. The underlying passive reduction mechanism is universal for any incident polarization. This work provides a viable solution for integrating wideband radiation with in-band stealth.

REFERENCES

[1] R. Ross, "Radar cross section of rectangular flat plates as a function of aspect angle," *IEEE Trans. Antennas Propag.*, vol. 14, no. 3, pp. 329-335, May 1966.

[2] M. U. Ullah, T. Bin Abdul Latef, M. Othman, M. I. Hussein, H. M. Alkhoori, Y. Yamada, K. Kamardin, and R. Khalid, "A progression in the techniques of reducing RCS for the targets," *Alex. Eng. J.*, vol. 100, pp. 153-169. Aug. 2024.

[3] H. Huang, A. A. Omar, and Z. Shen, "Low-RCS and beam-steerable dipole array using absorptive frequency-selective reflection structures," *IEEE Trans. Antennas Propag.*, vol. 68, no. 3, pp. 2457-2462, Mar. 2020.

[4] Y. Tian, W. Yao, X. Huang, W. Li, Y. Li and H. Yang, "Ultrawideband low-RCS copolarized beam-Scanning metantenna array," *IEEE Antennas and Wireless Propag. Lett.*, vol. 23, no. 10, pp. 2934-2938, Oct. 2024.

[5] X. Kong, L. Zhao, J. Liu, H. Song, and S. Zhang, "A low-frequency ultra-wideband absorber based on multi-mechanism collaborative design," *Sci. Sin. Inform.*, vol. 54, no. 12, pp. 2868–2880, Jan. 2024.

[6] X. Kong, S. Zhang, X. Pang, Y. Fu, L. Zhao, and Z. Shen, "Fast design of ultrawideband absorbers based on equivalent circuit model," *IEEE Antennas Wireless Propag. Lett.*, vol. 23, no. 6, pp. 1869–1873, Jun. 2024.

[7] R. Xu, X. Ma, X. Kong, S. Zhang, J. Liu, and L. Zhao, "An ultra-wideband metamaterial absorber with angular stability," *Appl. Comput. Electrom.*, vol. 39, no. 8, pp. 675–682, Aug. 2024.

[8] Y. Wen, S. W. Wong and Y. He, "A low RCS millimeter-wave antenna based on frequency selective absorber." *2024 IEEE International Workshop on Radio Frequency and Antenna Technologies (IWRFAT)*, pp. 14-16, May 2024.

[9] A. Sharma, S. Dwari, B. K. Kanaujia, D. Gangwar, S. Kumar, S.P. Singh, and A. Lay-Ekuakille, "In-band RCS reduction and isolation enhancement of a 24 GHz radar antenna using metamaterial absorber for sensing and automotive radar applications," *IEEE Sensors J.*, vol. 20, no. 21, pp. 13086-13093, Nov. 2020.

[10] Y. Zou, X. Kong, L. Xing, S. Jiang, X. Wang, H. Wang, Z. Liu, Y. Zhao, and J. Bornemann, "A slot antenna array with reconfigurable RCS using liquid absorber," *IEEE Trans. Antennas Propag.*, vol. 70, no. 7, pp. 6095–6100, Jul. 2022.

[11] Y. Han, L. Zhu, Y. Bo, W. Che and B. Li, "Novel low-RCS circularly polarized antenna arrays via frequency-selective absorber," *IEEE Trans. Antennas Propag.*, vol. 68, no. 1, pp. 287-296, Jan. 2020.

[12] Y. Liu, Y. Jia, W. Zhang and F. Li, "Wideband RCS reduction of a slot array antenna using a hybrid metasurface," *IEEE Trans. Antennas Propag.*, vol. 68, no. 5, pp. 3644-3652, May 2020.

[13] L. Zhu, J. Sun, G. Xu, Z. Hao and Q. Cao, "An integrated antenna array with broadband, low-RCS, and high-gain characteristics," *IEEE Trans. Antennas Propag.*, vol. 72, no. 6, pp. 5408-5413, Jun. 2024.

[14] Y. Deng, Y. Chen, H. Hu, Y. Yang, X. He and H. Ji, "A low-RCS antenna design with polarization conversion metasurfaces," *2021 IEEE 4th International Conference on Electronic Information and Communication Technology (ICEICT)*, pp. 196-198, Aug. 2021.

[15] Y. Shi, X. F. Zhang, Z. K. Meng and L. Li, "Design of low-RCS antenna using antenna array," *IEEE Trans. Antennas Propag.*, vol. 67, no. 10, pp. 6484-6493, Oct. 2022.

[16] J. Liu, J. Li, and Z. Chen, "Broadband polarization conversion metasurface for antenna RCS reduction," *IEEE Trans. Antennas Propag.*, vol. 70, no. 5, pp. 3834-3839, May 2021.

[17] L. Yin, P. Yang, Y. Gan, F. Yang, S. Yang and Z. Nie, "A low cost, low in-band RCS microstrip phased-array antenna with integrated 2-bit phase shifter," *IEEE Trans. Antennas Propag.*, vol. 69, no. 8, pp. 4517-4526, Aug. 2021.

[18] Z. Liu, W. Shao, X. Ding, B. Wang, L. Peng and Z. N. Chen, "Equivalent circuit-guided GAN sample generation of metasurface for low-RCS scanning array," *IEEE Trans. Antennas Propag.*, vol. 72, no. 9, pp. 7201-7210, Sept. 2024.

[19] P. Wang, Y. Jia, Y. Liu and W. Hu, "A wideband low-RCS circularly polarized reconfigurable C-shaped antenna array based on liquid metal," *IEEE Trans. Antennas Propag.*, vol. 70, no. 9, pp. 8020-8029, Sept. 2022.

[20] Y. Fan, J. Wang, Y. Li, J. Zhang, Y. Pang, Y. Han and S. Qu, "Low-RCS multi-beam metasurface-inspired antenna based on pancharatnam–berry phase," *IEEE Trans. Antennas Propag.*, vol. 68, no. 3, pp. 1899-1906, Mar. 2020.